Configurable Quasi-Optimal Sphere Decoding for Scalable MIMO Communications

Wu, Y., & McAllister, J. (2021). Configurable Quasi-Optimal Sphere Decoding for Scalable MIMO Communications. *IEEE Transactions on Circuits and Systems I: Regular Papers*, *68*(6), 2675 - 2687. https://doi.org/10.1109/TCSI.2021.3069639

Published in:
IEEE Transactions on Circuits and Systems I: Regular Papers

Document Version:
Peer reviewed version

Configurable Quasi-Optimal Sphere Decoding for Scalable MIMO Communications

Yun Wu, *Member, IEEE,* and John McAllister, *Senior Member, IEEE,*

Sphere Decoding (SD) enables real-time quasi-optimal symbol detection for Multiple-Input Multiple-Output (MIMO) communication systems via custom circuit accelerators. Configurable SDs allow accelerator cost to be balanced with detection accuracy for the most constrained MIMO environments, such as power-constrained Internet-of-Things (IoT) scenarios. However this high detection accuracy comes at high accelerator cost. This paper proposes a novel configurable SD which addresses this issue. A Robust Bounded Spanning with Fast Enumeration (R-BSFE) approach employs novel strategies for channel matrix pre-processing and symbol enumeration to maintain quasi-ML accuracy whilst reducing complexity by up to 74%. This enables accelerators for 802.11n on Xilinx FPGA with significantly lower cost and higher throughput. To the best of the authors' knowledge, the accelerators produced are the highest performance, lowest cost quasi-ML SD accelerators on record.

***Index Terms*—Field Programmable Gate Array (FPGA), Multiple-Input Multiple-Output (MIMO), Sphere Decoder, 802.11n**

I. Introduction

Multiple-Input Multiple-Output (MIMO) communications systems, as shown in Fig. 1, use multiple antennas at both transmitter and receiver to exploit spatial diversity and support unprecedented capacity and throughput [1]. MIMO is a foundation technology for modern wireless standards, such as LTE/LTE-Advanced [2], 802.11n/ac/ax [3] [4] [5], and 5G [6].

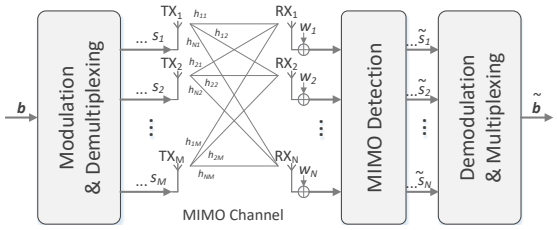

Fig. 1: MIMO Detection System Model

In the context of Internet-of-Things (IoT) systems, MIMO schemes can vary dramatically in their number of antennas, bit-to-symbol modulation density, operating environment and channel quality, energy budget and data rates [7]. For instance, 802.11ax permits MIMO configurations from 2×2 - 8×8 and modulation densities from QPSK - 1024-QAM.

Symbol detection is a key enabling MIMO technology [8]. Sphere Decoding (SD) [9] detectors make possible near-optimal real-time detection - well beyond linear equalization schemes such as Zero-Forcing (ZF) or Minimum Mean Square Error (MMSE) [10] - using custom circuit accelerators [11] [12]. These come in many forms including depth-first search (DFS) SD [13], List SD (LSD) [14], and Metric-First Search (MFS) [15]. Particularly notable are Breadth-First Search (BFS) approaches with fixed complexity, such as Fixed Complexity SD (FSD) [16] or K-Best [17], which offer deterministic parallel processing [18].

Bounded Selective Spanning with Extended Fast Enumeration (BSS-EFE) is the state-of-the-art BFS SD, allowing configuration for different IoT MIMO scales, detection accuracy and accelerator cost whilst avoiding the use of symbol list memory and sorting operators [19]. However, BSS-EFE suffers drawbacks which limit its efficiency:

- All SDs must tune the ordering of the MIMO channel matrix to their configuration; despite supporting any configuration, BSS-EFE does not account for this variation, reducing accuracy.
- The heuristics employed in BSS-EFE cannot identify the most likely symbols, further reducing accuracy and accelerator efficiency.
- To achieve highest accuracy, BSS-EFE accelerators incur very high cost relative to linear equalizers.

This paper addresses these issues. It proposes Robust Bounded Spanning with Fast Enumeration (R-BSFE) , an SD whose detection accuracy and cost can be configured at design-time. It makes the following contributions:

- A novel configuration approach is presented which improves detection accuracy by an average of 2 dB whilst reducing complexity by up to 42%.
- A channel matrix ordering approach is presented which adapts with the SD configuration to order the channel matrix for maximum detection accuracy. This is shown to increase accuracy by up to 5 dB or reduce complexity by up to 46.7%.
- FPGA accelerators for R-BSFE are shown to exhibit the same quasi-ML accuracy as BSS-EFE, but with increased throughput and cost reduced by up to 46%.

Sections IV - VI describe the proposed enumeration and pre-processing approaches and analyses their effect on detector accuracy and complexity. Section VII derives

Authors undertook this work at the Institute of Electronics, Communications and Information Technology (ECIT), Queen's University Belfast, UK e-mail: {ywu12, jp.mcallister}@qub.ac.uk

R-BSFE accelerators on Xilinx FPGA and compares their performance and cost to BSS-EFE.

II. Background

An $N_t \times N_r$ MIMO system assuming $N_t \leq N_r$ [20], shown in Fig. 1, modulates and multiplexes a bit stream $\mathbf{b}$ onto N_t transmit antennas to form a transmitted symbol vector $\mathbf{s} \in \mathbb{C}^{N_t \times 1}$. This is distorted by noise and multipath fading to form $\mathbf{y} \in \mathbb{C}^{N_r \times 1}$, retrieved by an N_r-antenna receiver. The relation between $\mathbf{s}$ and $\mathbf{y}$ is defined by (1)

$$\mathbf{y} = \sqrt{\frac{\rho}{N_r}} \cdot H \cdot \mathbf{s} + \mathbf{w} \tag{1}$$

where $\mathbf{w} \in \mathbb{C}^{N_r \times 1}$ is mutually independent and identically distributed complex Additive White Gaussian Noise (AWGN) with power σ_w^2. The Signal-to-Noise Ratio (SNR) ρ is given by $\frac{\sigma_s^2}{\sigma_w^2}$, where σ_s^2 the signal power of $\mathbf{s}$. The Rayleigh-distributed multipath channel is represented by $H \in \mathbb{C}^{N_r \times N_t}$ where $h_{i,j}$, represents the fading path between the i^{th} receive and j^{th} transmit antennas [21].

MIMO detectors derive an estimate $\tilde{\mathbf{s}}$ of the most likely value of $\mathbf{s}$ by seeking a solution amongst all possible transmitted symbol vectors such that[1] [22]:

$$\tilde{\mathbf{s}} = \arg\min_{\mathbf{x}_i} \|\mathbf{y} - H \cdot \mathbf{x}_i\|^2, \ \mathbf{x}_i \in D_{M_c}^{N_t}, \ i \in [1, M_c^{N_t}] \tag{2}$$

where M_c denotes the scale of modulation type, $D_{M_c}^{N_t} = \{\mathbf{x}_1, \mathbf{x}_2, \ldots \mathbf{x}_{M_c{}^{N_t}}\}$ denotes the set of all $M_c^{N_t}$ possible transmit symbol vectors over N_t transmit antennas.

The Maximum Likelihood (ML) detector establishes the upper bound on detection performance in terms of Bit Error Rate (BER) for uncoded MIMO detectors [23] by exhaustively considering all possible transmitted symbol vectors to determine the closest, in the Euclidean sense, to $\mathbf{y}$. However, the complexity of ML is $\mathcal{O}(M_c^{N_t})$. In modern wireless standards, both the number of antennas N_t and the size of the modulation dictionary M_c are increasing rapidly, and the associated exponential increase in complexity of ML detection is too large to allow it to be generally feasible in real-time.

A SD traverses a partial hypersphere in $D_{N_t}^C$ around the received symbol, evaluating each point according to:

$$\min_{\mathbf{x}} \|\mathbf{y} - H \cdot \mathbf{x}\|^2 \tag{3}$$

Via QR decomposition (3) can be expressed as [24]:

$$\min_{\mathbf{x}} \|R \cdot (\tilde{\mathbf{y}} - \mathbf{x})\|^2 \tag{4}$$

where $\tilde{\mathbf{y}}$ is a received symbol which has undergone ZF equalization, R is a upper-triangular matrix decomposed from $H = Q \cdot R$. Since R is upper-triangular, the final row of the product in (4) has a single non-zero entry, considered interference-free [25] and Euclidean distance can be calculated recursively row-by-row, in reverse order. At each row n are calculated the Partial Euclidean Distance (PED) and the Accumulated PED (APED), given by:

[1]Normalized QAM modulation is used throughout

$$PED_{nt} = \sum_{j=nt}^{N_t} r_{j,j}^2 \|\tilde{y}_j - x_j\|^2, \ nt \in [1, N_t] \tag{5}$$

$$APED_{nt} = \sum_{j=nt}^{N_t} PED_j \tag{6}$$

Intuitively, SD is a tree-search problem. As Fig. 2 shows, d is a radius around $\tilde{\mathbf{y}}$, the root, which limits the search by acting as an upper bound on the APED of leaf nodes [26]. The detected symbol is that amongst all the leaves with the lowest APED. Via careful choice of d and the search strategy [27], SD can provide quasi-ML accuracy, at much lower complexity than ML [28].

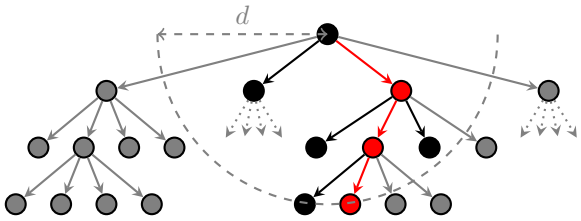

Fig. 2: Generic Tree-Search Structure of Sphere Decoder

Accelerators for SD use heuristics to achieve real-time processing. Despite work on DFS SD, such as radius reduction [29], and implementation with customized circuits [30], BFS is generally more effective in this regard. For instance, FSD uses a fixed tree shape which is a function of the number of transmit antennas. It enables quasi-ML accuracy and real-time detection [31] but is not configurable. K-best does permit configuration [32], allowing any number of symbols to be enumerated at each search tree level, but incurs costly sort operations in order to do so [33]. A K-best variant in [34] also mimics FSD in adopting a fixed tree structure for a given number of antennas and modulation scheme. Selective Spanning with Fast Enumeration (SSFE) avoids sort operations by employing a symbol enumeration heuristic, again enabling real-time detection [35] but has limited configurability. The promise of SSFE, though, led to the emergence of Boundary Selective Spanning with Extended Fast Enumeration (BSS-EFE) [19]. So far as the authors are aware, BSS-EFE is the state-of-the-art in configurable SD.

III. BSS-EFE

BSS-EFE allows any number of symbols to be enumerated at each layer of the search tree via a configuration vector $\mathbf{m} \in (\mathbb{Z}^+)^{N_t}$, where each $m_i \in \mathbf{m}$ defines the number of symbols enumerated at layer i of the tree. Fig. 3 shows an example BSS-EFE configuration.

A two-step detection process is followed. *Pre-processing* uses the Vertical Bell-laboratory Layer Space-Time (VBLAST) algorithm to determine $\tilde{\mathbf{y}}$, an equalized version of $\mathbf{y}$. It also orders the MIMO channel matrix H such that the i^{th} detected layer is determined by:

$$k_i = \arg \max_{nt=[1,N_t]} \mathbf{norm}_n \tag{7}$$

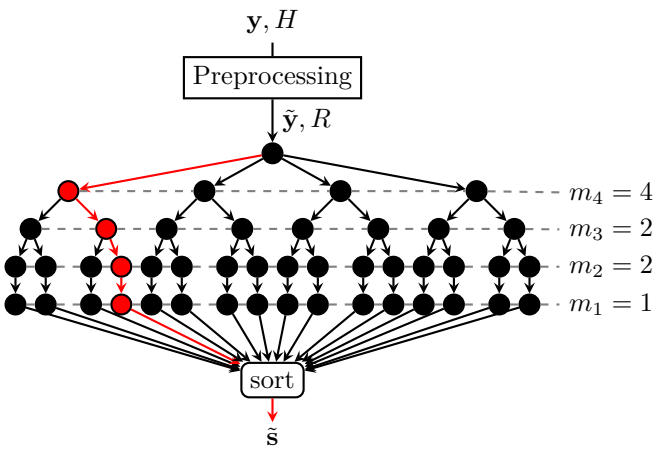

Fig. 3: $\mathbf{m} = [1, 2, 2, 4]$ BSS-EFE Structure

where $\mathbf{norm}_n$ is the norm of n^{th} column of H. This always orders the decoded signals from highest to lowest power.

The second *symbol enumeration* step - the tree search - is performed according to the order k. From each QAM symbol at the current layer i of the tree, m_{i+1} candidates are enumerated. The candidates selected are a subset $X = \{\widehat{x}_i\}_{i=2}^{M_c}$ identified using a fast enumeration heuristic:

$$\begin{aligned} \widehat{x}_0 &= \mathcal{Q}\left(\widehat{\tilde{y}}_{n,i}\right), \ i \in [1, M_c^{N_t}], \ n \in [1, N_t] \\ \widehat{x}_{k+1} &= \widehat{x}_k + z_1 \cdot (-1)^{w+1} \\ \widehat{x}_{l+1} &= \widehat{x}_l + z_2 \cdot (-1)^{w+1} \end{aligned} \tag{8}$$

where w, k, l and z_1 and z_2 are given by:

$$\begin{aligned} w &\in \left[1, \left\lceil \sqrt{m_i + 0.25} - 0.5 \right\rceil\right] \\ k &\in [(w-1) \cdot w + 1, w \cdot w] \\ l &\in [w \cdot w + 1, (w+1) \cdot w] \end{aligned} \tag{9}$$

$$\begin{aligned} z_1 &= sgn\left(\Re\left(d\right)\right) \cdot \phi + sqrt(-1) \cdot sgn\left(\Im\left(d\right)\right) \cdot (!\phi) \\ z_2 &= sgn\left(\Re\left(d\right)\right) \cdot (!\phi) + sqrt(-1) \cdot sgn\left(\Im\left(d\right)\right) \cdot \phi \end{aligned} \tag{10}$$

where $\mathcal{Q}(\bullet)$ denotes the QAM quantization, $d = \widehat{y}_n - \mathcal{Q}(\widehat{y}_n)$, and $\phi = \Re(d) > \Im(d)$.

To ensure that all enumerated symbols are in the valid QAM constellation set $\mathbf{\Omega}$ - a key differentiating factor between BSS-EFE and SSFE - a bounded spanning heuristic is employed. By introducing an enumerating bound,

$$\tau_u = \sqrt{M_c} - 1 \tag{11}$$

any $x_i \in \{\{|\Re(\widehat{x}_i)| > \tau_u\} \vee \{|\Im(\widehat{x}_i)| > \tau_u\}\}$ are offset:

$$x_i = x_i + \delta_i \qquad \text{for} \quad i = 1, \cdots, M_c \tag{12}$$

where δ_i is defined as

$$\begin{aligned} \delta_i = \ & -2 \cdot q_i \cdot \{(\Re(x_i) > \tau_u) \cdot \text{sgn}(\Re(x_0)) \\ & + j \cdot (\Im(x_i) > \tau_u) \cdot \text{sgn}(\Im(x_0))\} \end{aligned} \tag{13}$$

and

$$q_i = \left\lfloor \sqrt{m_i - 0.1} \right\rfloor + 1 \tag{14}$$

The final detected symbol vector $\mathbf{x}$ is chosen from all candidates according to:

$$\mathbf{x} = \arg\min_{\mathbf{x}_j}(APED_j), \ j \in [1, \prod_{i=1}^{N_t} m_i] \tag{15}$$

This enumeration heuristic selects symbols around $\tilde{y}$ as illustrated in Fig. 4 for $m_i = 15$ and 16-QAM. Valid QAM symbols are coloured blue and the sequence of symbols $\{\hat{s_0}, ..., \hat{s_{14}}\}$ labelled. A number of symbols, $\hat{s}'_4 - \hat{s}'_9$, are known to be outside the valid constellation and are projected via (12) onto valid alternatives.

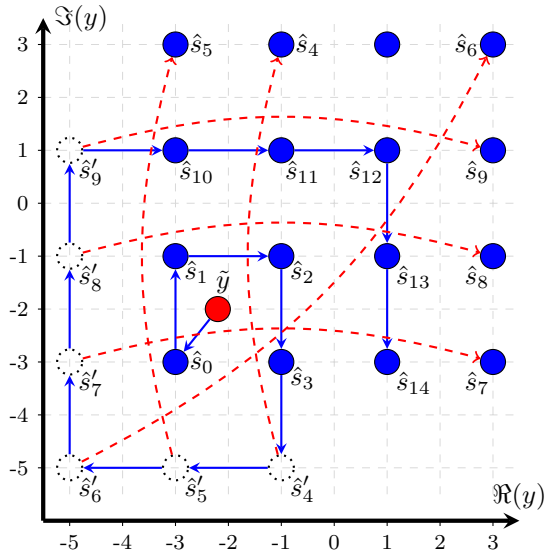

Fig. 4: BSS-EFE Enumeration Process

This heuristic enables fast enumeration but potentially limits detection accuracy. Fig. 4 shows that the symbols enumerated are not necessarily the most likely. For instance, in Fig. 4, $\hat{s}'_6$ is enumerated before $\hat{s}'_7$ and $\hat{s}'_8$, despite the latter two being more likely by virtue of being closer to $\tilde{y}$ in the Euclidean sense. If only six symbols had been enumerated in this example, $\hat{s}'_6$ would be included in place of these more likely alternatives. The bounded spanning heuristic can also lead to the same issue - $\hat{s}_6$ is less likely than the point $1 + 3j$, but is nevertheless preferred.

A second issue is pre-processing. VBLAST orders antennas for detection in reverse order of distortion [21], [36]. FSD, however, has shown that if full enumeration is used for the early layers, reversed VBLAST order is provably optimal. Since BSS-EFE can enumerate any number of symbols at each layer, either V-BLAST or FSD ordering is most appropriate, depending on the value of $\mathbf{m}$.

Sphere Decoders offer much higher detection accuracy than simple linear equalizers, at the cost of much more expensive accelerators. Some cost increase is unavoidable since equalization is a sub-operation of SD, alongside channel matrix ordering and tree search. It is desirable to minimise the overhead of the latter two operations to offer MIMO systems the highest possible detection accuracy at the lowest possible cost. The inefficiencies in the BSS-EFE heuristics outlined above lead to lower efficiency

accelerators, negatively impacting their performance or their cost. To produce higher efficiency configurable SD accelerators, there are three key requirements:

- **Enumeration**: enumerating the most likely subset of possible symbols.
- **Bounding**: mapping known-impossible symbols to the most likely, valid alternatives.
- **Pre-processing**: defining a channel matrix ordering approach accounting for $\mathbf{m}$.

This paper addresses these requirements. Only 'hard' detection is considered, on the basis these are the foundation for 'soft' alternatives. Various MIMO scales 2×2 - 8×8 and QPSK - 64QAM are considered to represent the diversity of modern wireless IoT systems.

IV. Robust Fast Enumeration

BSS-EFE enables low-cost custom accelerators by limiting the number of symbols enumerated whilst avoiding sort, square root or comparison operations. It does not, however, always enumerate the most likely set of symbols. An ideal alternative would resolve the latter shortcoming, whilst maintaining the former benefit.

Theoretically, the real and imaginary parts of each complex-valued received symbol are orthogonal, and can be considered separately during detection [37]. This is realised using a system model based on Real-Value Decomposition (RVD) [38], given by (16).

$$\begin{aligned}\tilde{\mathbf{y}} &= \begin{bmatrix} \Re(\mathbf{y}) \\ \Im(\mathbf{y}) \end{bmatrix} \\ &= \begin{bmatrix} \Re(H) & -\Im(H) \\ \Im(H) & \Re(H) \end{bmatrix} \cdot \begin{bmatrix} \Re(\mathbf{s}) \\ \Im(\mathbf{s}) \end{bmatrix} + \begin{bmatrix} \Re(\mathbf{w}) \\ \Im(\mathbf{w}) \end{bmatrix} \\ &= \tilde{H} \cdot \tilde{\mathbf{s}} + \tilde{\mathbf{w}}\end{aligned} \tag{16}$$

Fig. 5 illustrates the effect of considering a complex symbol as two real-valued components on the structure of an SD tree. In Fig. 5a, four complex symbols are enumerated. This equates to the two-layer structure in Fig. 5b, where each layer enumerates the real and imaginary components of $\tilde{y}$ in turn. The number of APEDs in Fig. 5b is larger but since each operates on real-valued data only, by separating the two components, the second gives more fine-grained control of the SD tree structure.

The configuration vector $\tilde{\mathbf{m}} \in \mathbb{R}^{2\times N_t}$ where each $\tilde{m}_j \in \tilde{\mathbf{m}}$ represents the number of real symbols enumerated at layer j in the detection tree. During breadth-first search, the k^{th} candidate $\tilde{x}_{j,k}$ enumerated at the j^{th} tree search layer is identified via a heuristic which derives a sequence of candidate real symbols, $\tilde{\mathbf{X}} = \{\tilde{x}_{j,k}\}_{j=1}^{\tilde{m}_j}$ using (17)

$$\tilde{x}_{j,k} = \tilde{x}_{j,1} + (step \cdot dir \cdot sdist)\,,\ k \in \left[2, \sqrt{M_c}\right] \tag{17}$$

where

$$step = d\,\lfloor k/2 \rfloor\,, \tag{18}$$

$$sdist = 2 \cdot sign(\tilde{y}_j - \tilde{x}_{j,1}), \tag{19}$$

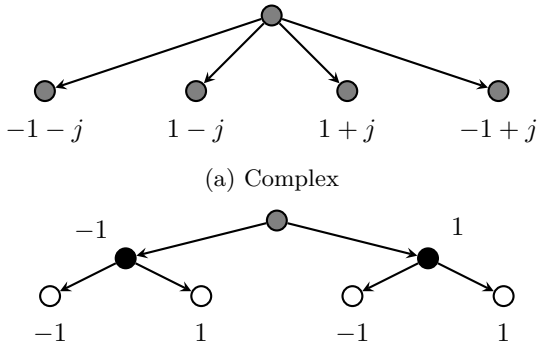

Fig. 5: Complex and Real Tree Structures

and

$$dir = \begin{cases} -1 & k \text{ is odd} \\ 1 & k \text{ is even} \end{cases} \tag{20}$$

Fig. 6 illustrates the behavior of the enumeration scheme on a normalized scale for QAM. Note that, since the values considered are real, the sequence traverses a one-dimensional line, rather than a two-dimensional plane in Fig. 4 for BSS-EFE. Each component of the QAM symbol takes values $\tilde{\mathbf{\Omega}} = \{-3, -1, 1, 3\}$. The equalized symbol $\tilde{y}$ is quantized to the closest value - respectively -3 and -5 for the values of $\tilde{y}$ in Fig. 6a and Fig. 6b. The sequence of enumerated symbols is as illustrated.

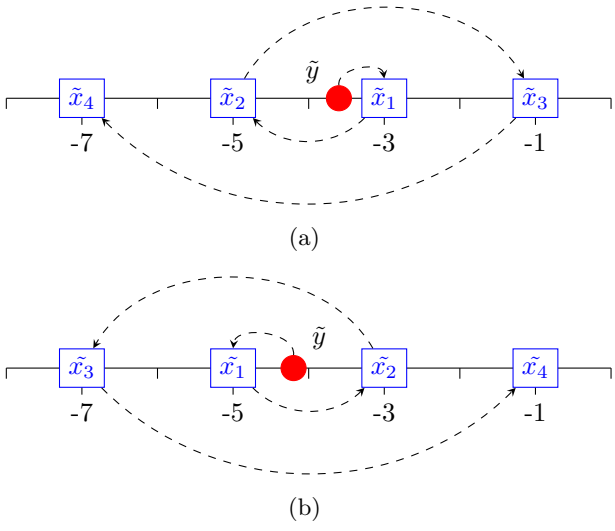

Fig. 6: Example of 4 Real Symbols Fast Enumerations

This Real-valued Fast Enumeration (RFE) heuristic leads to detection accuracy as compared to the EFE heuristic in BSS-EFE in Fig. 7. There are a number of significant observations. Values for SNR of less than 12 dB are not reported, since in this range performance variation is imperceptible. At higher SNR values, the accuracy of the RFE detector is superior. The peak gain is 2dB SNR, using RFE-$[1, 1, 1, 1, 1, 1, 1, 2]$ for QPSK; the average gain is 0.8 dB.

When realised using, for example, full custom hardware, programmable logic, or even software, there is no consis-

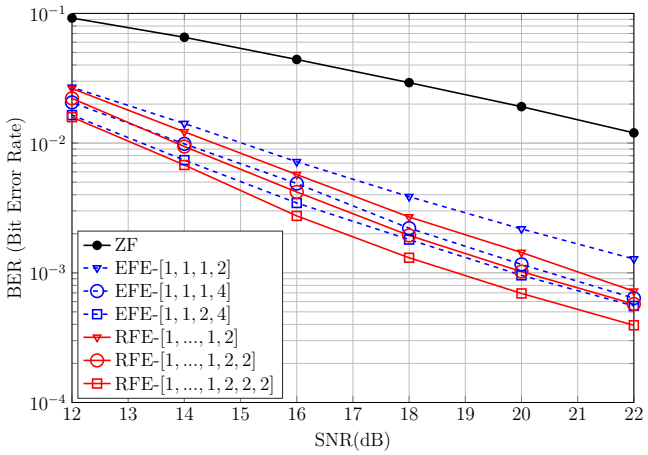

(a) QPSK

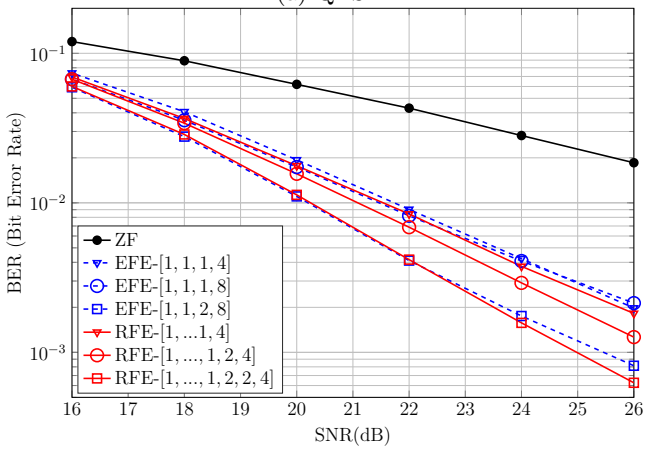

(b) 16-QAM

Fig. 7: RFE v.s. EFE Detection Accuracy

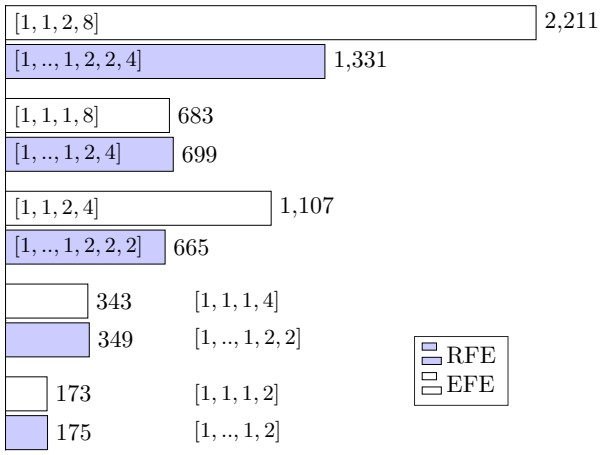

Fig. 8: RFE v.s. EFE Complexity Comparison

Fig. 9. This describes the results of a Monte-Carlo simulation applying RFE to 10^5 symbols for each value of SNR $0-40$ dB. The proportion of invalid symbols decreases with SNR until about 20 dB is reached. The minimum proportion of invalid symbols for all other QAM constellation sizes and number of enumerated symbols is around 20%. This is a significant proportion of all symbols.

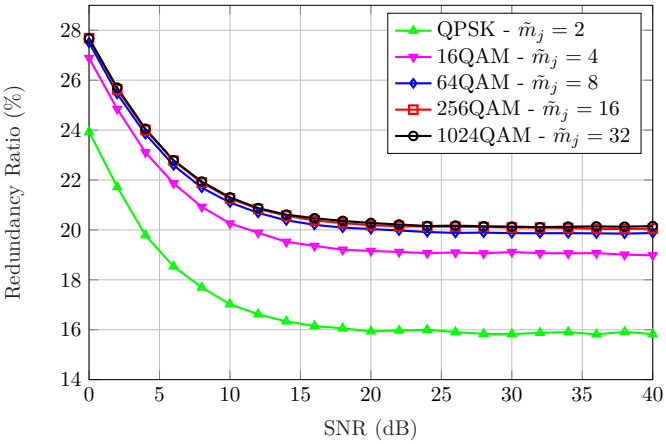

Fig. 9: Redundant Symbol Enumeration in RFE Heuristic

tent unit of complexity via which to compare different algorithms. Hence, different SD algorithms are compared here by comparing the numbers of operations of the same type (additions, multiplications) each incurs. For each of the configurations in Fig. 7, Fig. 8 compares the number of arithmetic operations required. Two trends are evident: in three of the comparisons, the marginally superior accuracy of RFE comes at the cost of complexity increases of up to 2.3%. However, two of the configurations illustrate the real potential of RFE, combining increased accuracy with complexity reductions by 39.8% and 39.9%. Except for the specific configurations where EFE enumerates more than one symbol at a single layer, RFE enables increased accuracy at much-reduced complexity.

V. Robust Bounded Spanning

The benefits of RFE can be further amplified by ensuring invalid symbols are not enumerated. For instance, the enumeration paths in Fig. 6 include -5 and -7, which are known not to occur. If symbols within the valid set were enumerated instead of these symbols, such as 1 in both examples, detection accuracy may be increased.

The proportion of invalid symbols enumerated by RFE, given the enumeration bound in (11), is illustrated by

A Robust Bounded Spanning (RBS) approach is proposed to identify a valid alternative for every invalid symbol. There are three challenges in doing so:

1) The alternatives should not enumerate symbols which would otherwise be enumerated by the RFE heuristic.
2) The most likely symbols should be enumerated.
3) Primitive arithmetic/logical operations are preferred.

RBS compares every enumerated symbol with a boundary τ_u defined by the size of the modulation dictionary, as in (11). This defines an offset $offset_{j,k}$ for $k \in [2, \sqrt{M_c}]$ enumerated symbols at j^{th} antenna using (21):

$$offset_{j,k} = \begin{cases} -dist \cdot sgn, & |\tilde{x}_{j,k}| > \tau_u \\ 0 & \text{otherwise} \end{cases} \tag{21}$$

where $dist = 2 \cdot \tilde{m}_j$ is a scaling factor and sgn the sign of the first quantized symbol $sign(\tilde{x}_{j,1})$. This offset is adding to symbols outside the known valid region $\tilde{\mathbf{\Omega}}$.

The effect of this bounding process is illustrated in Fig. 10 for the RFE-enumerated sequence in Fig. 6a. For 16 QAM, by (11), $\tau_u = 3$. Hence, of the sequence of enumerated symbols $\{-3, -5, -1, -7\}$ both $\tilde{x}_{j,2} = -5$ and $\tilde{x}_{j,4} = -7$ are known to be invalid, since they fall outside the bound. According to (21), the offsets for each of these is 8, with the respective updated symbols taking the values $\tilde{x}_{j,2} = 3$ and $\tilde{x}_{j,4} = 1$. Hence, $\tilde{x}_{j,2}$ and $\tilde{x}_{j,4}$ are mapped to valid symbols in $\tilde{\mathbf{\Omega}}$, which would not otherwise have been enumerated. Note that, whilst the symbols are not enumerated in monotonically decreasing order of likelihood, the reliance of (21) on $\tilde{m}_j$ ensures that the closest set is enumerated; for instance, were $\tilde{m}_j = 2$, the enumerated sequence would be $\{-3, -1\}$.

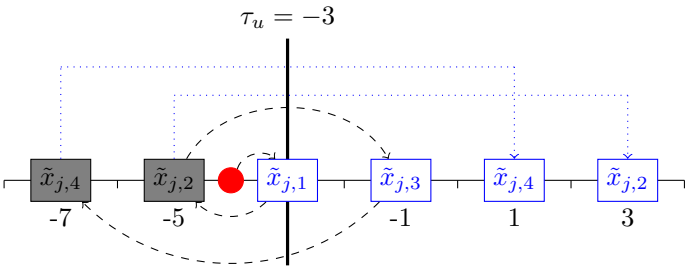

Fig. 10: Bounded Offset Enumeration

The PED and APED metrics for candidate selection, $P\tilde{E}D$ and $A\tilde{PED}$, are calculated using (22) and (23).

$$P\tilde{E}D_{l,k} = \sum_{j=l}^{N_t \times 2} \tilde{r}_{j,j}^2 \left\| \tilde{y}_j - \underline{\tilde{x}}_{j,k} \right\|^2, \; l \in [1, N_t \times 2] \tag{22}$$

$$A\tilde{PED}_{l,k} = \sum_{j=l}^{N_t \times 2} P\tilde{E}D_{j,k} \tag{23}$$

where $\tilde{y}_j$ is the j^{th} element of $\tilde{\mathbf{y}}$; $\tilde{x}_{j,k}$ is the k^{th} symbol enumerated at the j^{th} layer; l is the index of current layer. The resulting symbol vector $\tilde{\mathbf{x}}$ is given by:

$$\tilde{\mathbf{x}} = \arg\min_{\tilde{\mathbf{x}}_\mathbf{j}} (A\tilde{PED}_j), \; j \in [1, \prod_{nt=1}^{N_t \times 2} \tilde{\mathbf{m}}_{nt}] \tag{24}$$

The resulting $\tilde{\mathbf{x}}$ is reordered and multiplexed into single data stream and demodulated into detected bits.

The effect of RBS on detection accuracy is shown in Fig. 11, which compare R-BSFE (i.e. the combined RFE and RBS heuristics) with BSS-EFE for QPSK and 16-QAM, 4×4 MIMO schemes. In all cases, detection performance is similar. However, this is in the context of potentially very different complexity requirements. Fig. 12 compares the complexity of the configurations from Fig. 11.

In all cases BSS-EFE is at least as complex as R-BSFE and in several cases R-BSFE enables the same accuracy

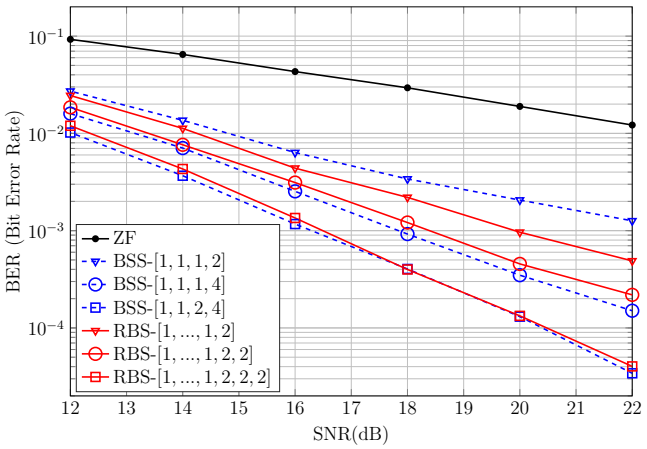

(a) QPSK

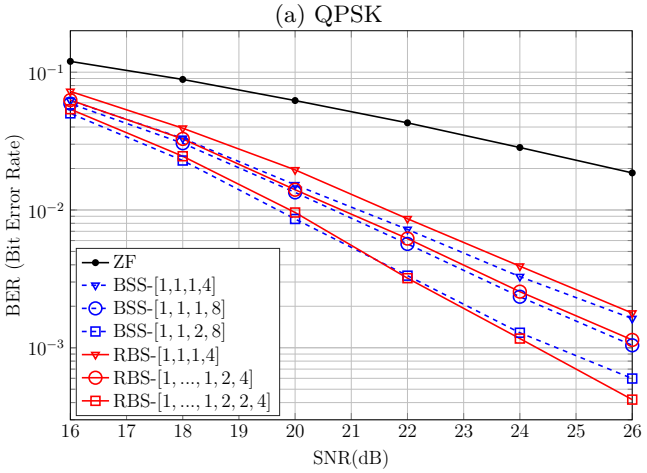

(b) 16-QAM

Fig. 11: RBS v.s. BSS Performance Comparison

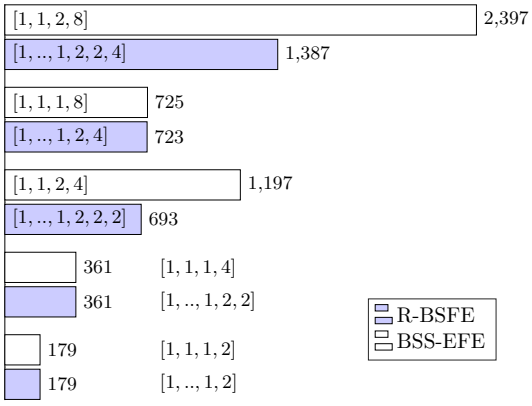

Fig. 12: RBS v.s. BSS Complexity Comparison

with much lower complexity. Fig. 11b shows that R-BSFE-$[1, 1, 1, 1, 1, 2, 2, 4]$ has almost identical accuracy to BSS-EFE-$[1, 1, 2, 8]$, but 42.1% lower complexity. Similarly, R-BSFE-$[1, 1, 1, 1, 1, 2, 2, 2]$ is as accurate as BSS-EFE-$[1, 1, 2, 4]$, but is 42.1% simpler. The proposed bounded spanning and fast enumeration schemes can significantly reduce complexity whilst maintaining detection accuracy.

Table I briefly summarises the enumeration differences between SSFE, BSS-EFE and R-BSFE.

TABLE I: Enumeration Method Comparison

	Pros & Cons
SSFE	redundant complex symbol enumeration, limited performance with least complexity
BSS-EFE	non-redundant complex symbol enumeration, better performance with most complexity
R-BSFE	non-redundant real symbol enumeration, improved performance with reduced complexity

VI. Pre-Processing

Depending on the topology of the search tree, different orderings of the channel matrix lead to highest detection accuracy. V-BLAST orders antennas for decoding in decreasing order of the level of distortion experienced by each transmit antenna. FSD uses reversed-VBLAST order and full enumeration of all possible symbols initially, before reverting to V-BLAST order after a number of antennas - $NFS = \lceil \sqrt{N_t} - 1 \rceil$ for complex FSD PP [16] or $NFS = \lceil \sqrt{2 \cdot N_t} - 1 \rceil$ for real-valued FSD [39].

Since R-BSFE can achieve any configuration it needs to adapt its ordering, based on $\tilde{\mathbf{m}}$ to use FSD in some configurations and V-BLAST in others. A real-valued pre-processing technique is proposed to distinguish these. The received symbol vector $\mathbf{y}$ is divided into real and imaginary parts and QR decomposition of $\tilde{H}$ is performed to obtain the upper triangular matrix $\tilde{R}$, as shown in (25).

$$\tilde{H} = \tilde{Q} \cdot \tilde{R}, \tag{25}$$

According to the norm of each column of $\tilde{H}$, iterative permutation is applied during QR decomposition. The objective is to determine the number of antennas for which VBLAST permutation is applied, before reverse-VBLAST ordering is applied for the remainder. This approach generalises FSD ordering. It does not pre-define the number of layers of each depending on the number of antennas, as in FSD, but instead applies V-BLAST only in cases where full enumeration occurs. Specifically, the R-BSFE channel ordering follows (26):

$$\tilde{k}_i = \begin{cases} \arg\max_{nt=[1,2\times N_t]} \mathbf{no\tilde{r}m}_{nt}, & \tilde{m}_j < \sqrt{M_c} \\ \arg\min_{nt=[1,2\times N_t]} \mathbf{no\tilde{r}m}_{nt}, & \tilde{m}_j \geq \sqrt{M_c} \end{cases} \tag{26}$$

where $\mathbf{no\tilde{r}m}_{nt} = \left\|\tilde{H}\right\|$, $\tilde{\mathbf{m}}$ is the configuration vector in real domain and $\tilde{m}_j$ the number of candidates to enumerate at j^{th} layer.

This approach has two 'phases' - first, antennas are detected in increasing order of received signal quality, and then the order is reversed. This is the same approach employed in FSD. However (26) does not define the boundary between these two phases in terms of the number of antennas, rather the size of the modulation dictionary. When the number enumerated reaches the real constellation size, $\sqrt{M_c}$, the ordering chooses the transmitter with the lowest **norm**. According to $\tilde{m}_j$ it maintains the optimal VBLAST order, with decreasing transmit power, when fewer than $\sqrt{M_c}$ symbols are enumerated. Note that $\sqrt{M_c}$ can be calculated off-line. The difference between these approaches is summarised in Table II.

TABLE II: PP Ordering Summery

	Order of Channel Matrix
VBLAST	Highest to lowest transmitting antenna power
FSD	Reversed VBLAST ordering for first NFS antennas, VBALST ordering for $N_t - NFS$ antennas
R-BSFE	Reversed VBLAST ordering whenever $\tilde{m}_j \geq \sqrt{M_c}$, VBLAST ordering whenever $\tilde{m}_j < \sqrt{M_c}$

Fig. 13 shows the performance of R-BSFE ($\tilde{\mathbf{m}} = [1,1,1,1,1,4,2,4]$) when FSD, VBLAST or the proposed ordering approach is used. Performance is poorest with FSD due to the reverse-VBLAST ordering of the non-full search layers. The proposed ordering is superior to VBLAST due to the adaptive reverse-VBLAST ordering.

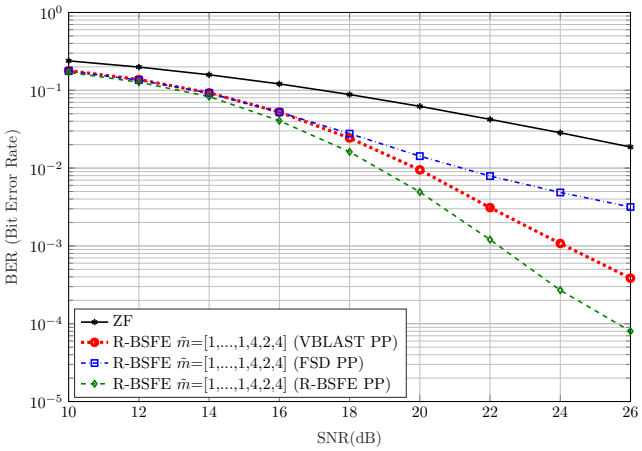

Fig. 13: R-BSFE 16-QAM 4x4 with Different PP

The accuracy of R-BSFE using the proposed ordering approach is compared to BSS-EFE in Fig. 14. A maximum SNR gain of 5 dB is achieved for QPSK under 4×4 MIMO in Fig. 14b, and 2 dB SNR for 16-QAM. There is a clear accuracy benefit to employing the proposed scheme over solely FSD or V-BLAST.

VII. R-BSFE: Performance and Cost

A. Detection Accuracy

The accuracy of R-BSFE in various configurations for 2×2, 4×4 and 8×8 MIMO, employing QPSK, 16-QAM and 64-QAM, is described, alongside comparable BSS-EFE configurations, K-Best and FSD in Fig. 15 - 17.

A number of trends are apparent when BSS-EFE (solid lines) and R-BSFE (dashed lines) are compared in pairs. When QPSK is employed, in each of Fig. 15a, 16a and 17a, the accuracy of R-BSFE is generally superior to BSS-EFE. This is despite R-BSFE enumerating no more QAM symbols, ultimately, than the BSS-EFE equivalent. For instance R-BSFE-$[1,1,1,1,2]$ offers 1 dB accuracy gain relative to BSS-EFE-$[1,2]$ for 2×2 QPSK MIMO, with the other pairs in Fig. 15a offering near-identical accuracy.

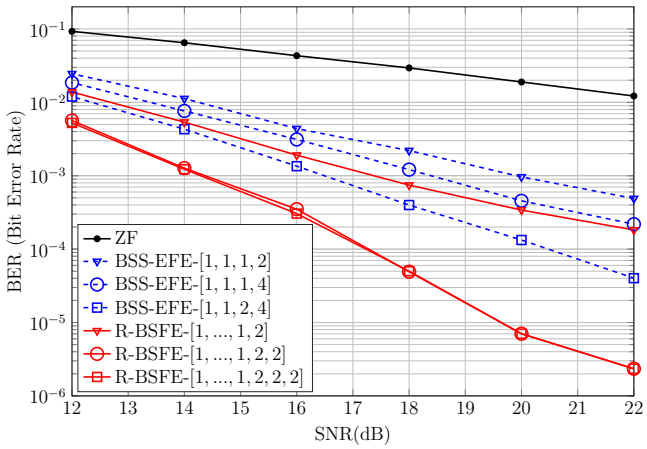

(a) QPSK

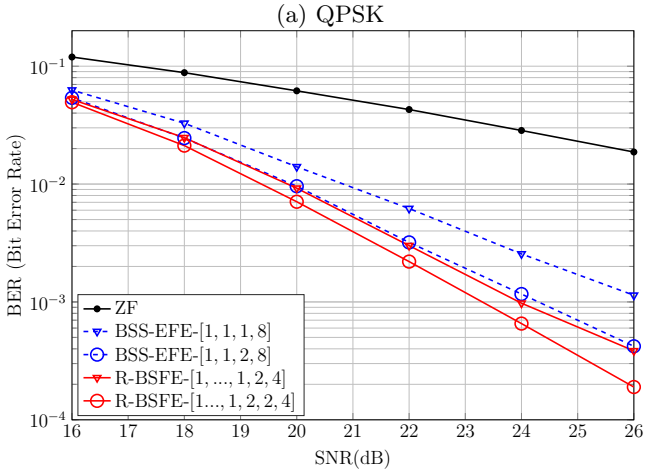

(b) 16-QAM

Fig. 14: R-BSFE Pre-Processing Accuracy Comparison

This benefit is repeated for 4×4 and 8×8 MIMO, with R-BSFE accuracy gains increasing with number of antennas. For instance, in 8×8, QPSK MIMO, R-BSFE-$[1, ...1, 2, 2, 2]$ offers 3 dB gain over BSS-EFE-$[1, ..., 1, 2, 4]$. R-BSFE generally offers superior accuracy.

For the same MIMO topologies, as modulation density increases (between adjacent figures), BER performance converges. However, R-BSFE is generally increasingly superior to BSS-EFE as the number of antennas increase. In only two cases is R-BSFE accuracy inferior to BSS-EFE.

A series of K-BEST configurations ($K = \{2, 4\}$ for QPSK, $K = \{4, 8\}$ for 16-QAM and $K = \{8, 16\}$ for 64-QAM) are compared to R-BSFE. For larger K, performance is comparable to R-BSFE with the most complex configurations; there is no significant difference for small numbers of antennas but the performance of complex K-BEST configurations grows with number of antennas when SNR is low in Fig. 17a-17c. The same trend exists for increasing the QAM density. The lowest SNR values reported for QPSK, 16-QAM and 64-QAM are 6 dB, 14 dB and 22 dB. For 16-QAM and 64-QAM, below these values (the majority of practical scenarios) accuracy is largely indistinguishable. Since BSS-EFE offers quasi-ML accuracy, this is a benefit of R-BSFE - the motivation for R-BSFE is to maintain this accuracy at reduced cost.

B. Complexity

The complexity of the detectors compared in Figs. 15 - 17 are illustrated in Fig. 18 - 20. The figures pair together the R-BSFE and BSS-EFE schemes whose number of enumerated symbols are closest. A series of trends are evident. For 2×2 and 4×4 MIMO topologies, the R-BSFE variant incurs slightly reduced computational complexity, whilst generally also enabling superior detection accuracy. However, in all 8×8 configurations, these are accompanied by increases in complexity; when the most accurate R-BSFE and BSS-EFE options are compared for the former incurs complexity increases of 4.1%, 4.0% and 4.2% for QPSK, 16-QAM and 64-QAM respectively.

However, comparison of complexity for the same or improved cost is more appropriate since R-BSFE makes possible configurations with cost/accuracy balances which BSS-EFE could not. The benefit of this control is demonstrated by comparing a variety of R-BSFE and BSS-EFE configurations. In the 8×8 64-QAM case, R-BSFE-$[1, ...1, 2, 8]$ is the most accurate algorithm and incurs greatest complexity. But when compared with BSS-EFE-$[1, ..., 1, 2, 16]$ - the most accurate BSS-EFE configuration - even R-BSFE-$[1, .., 1, 8]$ offers superior accuracy, yet incurs only 26.3% of the complexity. Hence, the increased configurability of R-BSFE can offer either very significant reductions in complexity, increases in accuracy, or both.

Besides BSS-EFE, FSD and K-BEST are compared over all BSS-EFE and R-BSFE cases. As shown in Fig. 15-17, FSD has the best detection performance. Compared to the most accurate R-BSFE, complexity at low antenna number such as 2×2 and 4×4 is even lower. However, it exceeds R-BSFE exponentially as the antenna number and QAM density increase. K-BEST with large K configuration is of similar complexity to the most accurate R-BSFE for QPSK which is slightly lower as antenna number grows. However, as the QAM density grows, it exceeds R-BSFE significantly as antenna numbers increase. The 1 dB performance gain over R-BSFE is at the cost of at least twice the complexity for 16-QAM and over an order of magnitude greater complexity for 64 QAM, as shown in Fig. 20b and Fig. 20b.

VIII. Accelerator Architecture

This section evaluates the effect of the complexity reductions enabled by R-BSFE on the performance and cost of FPGA accelerators. The results are compared with the state-of-the-art electronic system level implementations of BSS-EFE, K-BEST with similar detection performance, and FSD with similar tree-search breadth.

All accelerators are created using the FPGA Processing Element (FPE) employing 16-bit (10 fractional bits) fixed-point arithmetic. Built around the on-chip DSP slices on Xilinx FPGA, these realise additions and multiplications using hardened components with the same latency. They are all automatically derived to realise a single R-BSFE

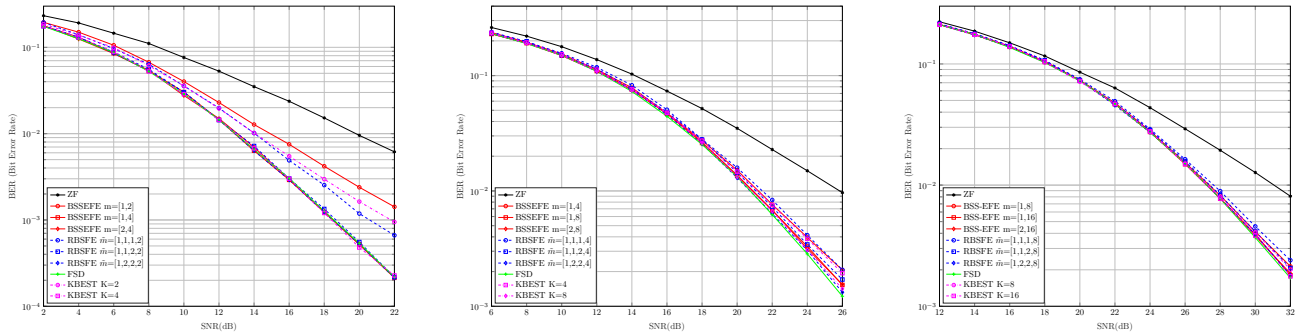

(a) QPSK (b) 16 QAM (c) 64 QAM

Fig. 15: Performance Comparison: R-BSFE v.s. BSS-EFE, K-BEST and FSD, 2×2 MIMO

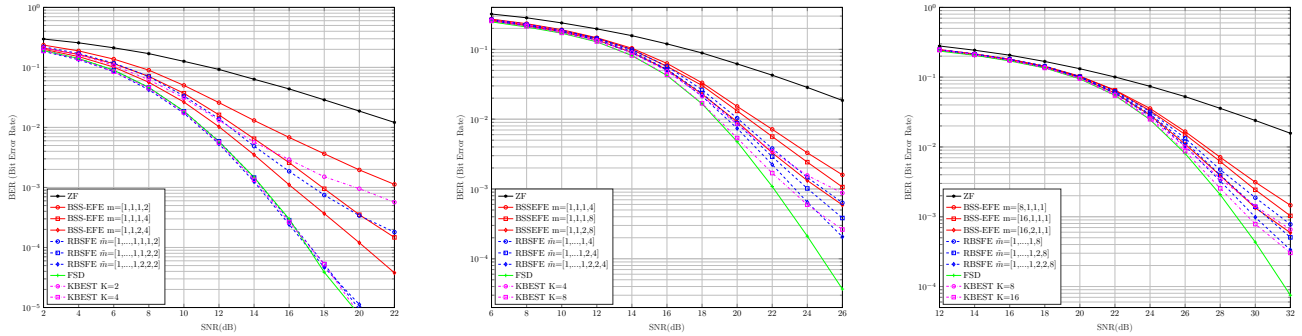

(a) QPSK (b) 16 QAM (c) 64 QAM

Fig. 16: Performance Comparison: R-BSFE v.s. BSS-EFE, K-BEST and FSD, 4×4 MIMO

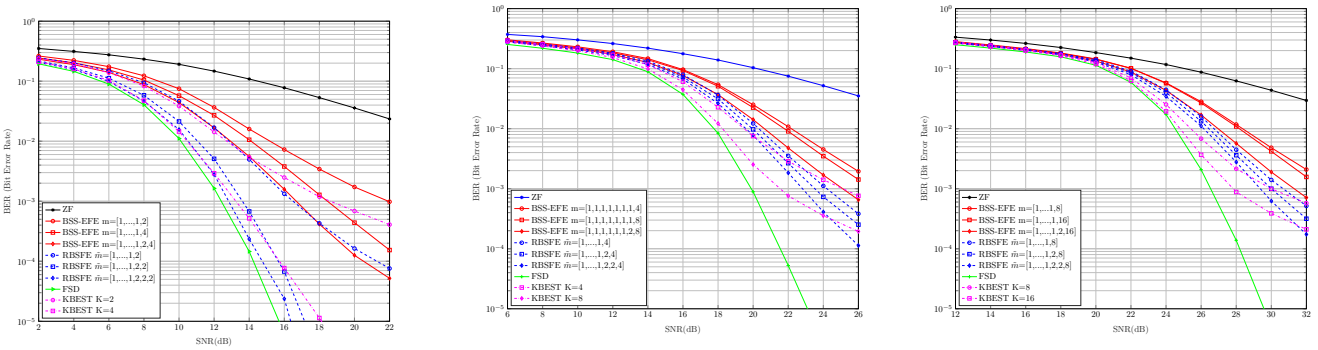

(a) QPSK (b) 16 QAM (c) 64 QAM

Fig. 17: Performance Comparison: R-BSFE v.s. BSS-EFE, K-BEST and FSD, 8×8 MIMO

configuration using the process described in [40] to meet the throughput constraints of 802.11n, for controlled comparison with [41]. An example accelerator for 16-QAM, 2×2, $\tilde{m} = [1, 1, 2, 4]$ R-BSFE is shown in Fig. 21.

The R-BSFE tree structure for the configuration is shown in Fig. 21a; $T_1 - T_4$ are enumeration and APED calculations, while T_5 identifies the solution with minimum APED. The work in [41] demonstrates that high-performance, efficient accelerators for SD can be enabled by using networks of fine-grained SIMD processors; this was extended in [40] to demonstrate how such accelerators can be automatically synthesised from a task graph such as that in Fig.21a. In the case of Fig.21b, this results in five SIMD processors: a single 10-lane SIMD, three 15-lane SIMDs and a single 5-lane SIMD, where 30 symbols (OFDM sub-carriers) are processed concurrently.

Section VII-A showed that in general, R-BSFE has the same or superior accuracy to BSS-EFE, with gains increasing with the number of antennas. Tables III and IV describe the accuracy and cost of the detectors quoted

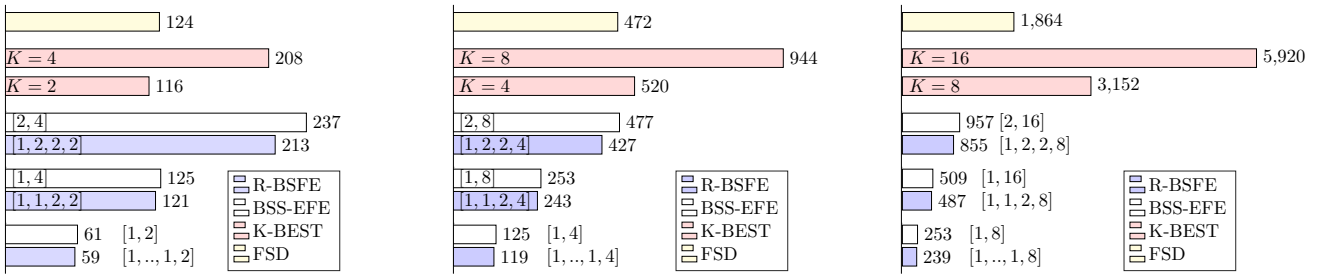

(a) QPSK (b) 16-QAM (c) 64-QAM

Fig. 18: Complexity Comparison: R-BSFE v.s. BSS-EFE, K-BEST and FSD, 2×2 MIMO

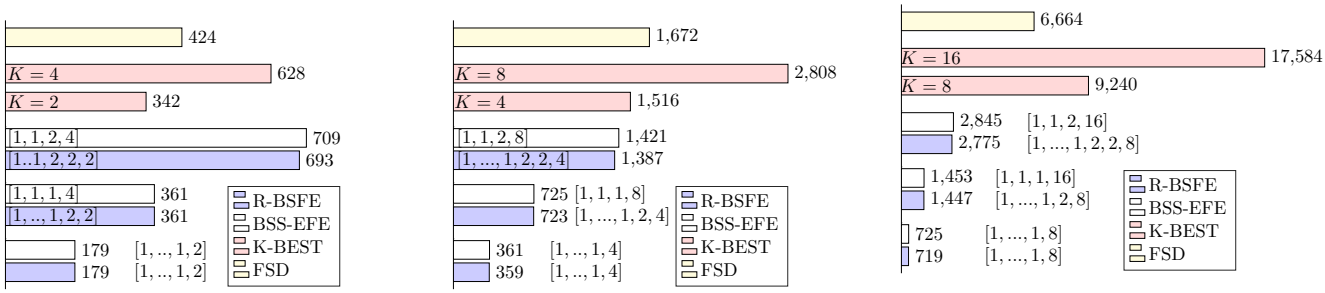

(a) QPSK (b) 16-QAM (c) 64-QAM

Fig. 19: Complexity Comparison: R-BSFE v.s. BSS-EFE, K-BEST and FSD, 4×4 MIMO

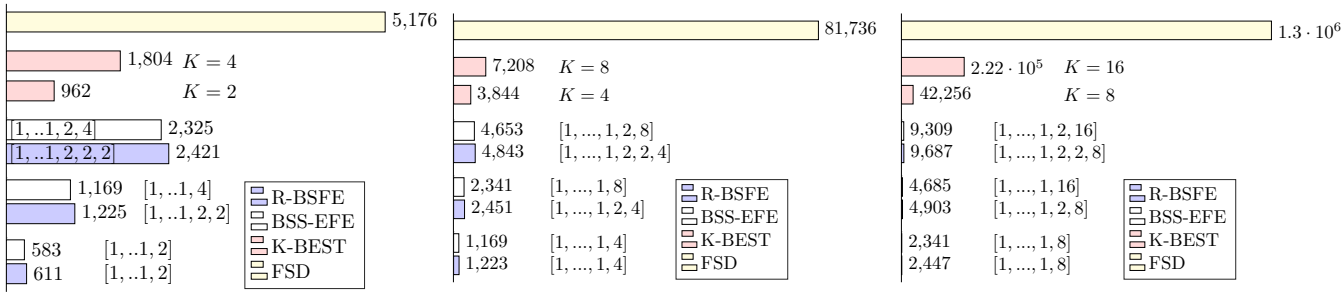

(a) QPSK (b) 16-QAM (c) 64-QAM

Fig. 20: Complexity Comparison: R-BSFE v.s. BSS-EFE, K-BEST and FSD, 8×8 MIMO

in Fig. 15a and 15b for 802.11n MIMO.

TABLE III: Resource Comparison: R-BSFE v.s. BSS-EFE and BFSD, 2×2, QPSK

	BFSD [34]	BSS-EFE [41]			R-BSFE		
Configuration	N/A	[1,2]	[1,4]	[2,4]	[1,1,1,2]	[1,1,2,2]	[1,2,2,2]
DSP48E1	22	24	24	56	18	28	49
LUT ($\times 10^3$)	1.3	3.6	3.8	7.9	2.8	4.7	7.8
Clock (MHz)	125	362	361	351	377	369	370
T (Mbps)	125.6	122.0	123.0	133.9	138.6	125.6	126.3

In Table III, R-BSFE-$[1, 1, 1, 2]$ offers superior accuracy and throughput to BSS-EFE-$[1, 2]$, at increased cost. In this configuration, BSS-EFE enumerates relatively few symbols and is quite efficient. However as BSS-EFE becomes more complex, R-BSFE becomes more effective. R-BSFE-$[1, 1, 2, 2]$ sees a mild increase in LUT cost relative to BSS-EFE-$[1, 4]$, alongside mild throughput increases for the same detection accuracy. R-BSFE-$[1, 2, 2, 2]$ enables an 11% reduction in DSP48E1, alongside a 4% increase in LUT over BSS-EFE-$[2, 4]$, whilst also enabling a throughput increase. The FSD and BFSD implementations in Table III consume less LUT but more DSP than R-BSFE-$[1, 1, 1, 2]$, with slightly better throughput.

TABLE IV: Resource Comparison: R-BSFE v.s. BSS-EFE and BFSD, 2×2, 16-QAM

	BFSD [34]	BSS-EFE [41]			R-BSFE		
Configuration	N/A	[1,4]	[1,8]	[2,8]	[1,1,1,4]	[1,1,2,4]	[1,2,2,4]
DSP48E1	84	24	63	70	24	60	70
LUT ($\times 10^3$)	2.9	3.8	11.5	14.0	4.6	13.0	12.2
Clock (MHz)	271	361	337	343	370	351	346
T (Mbps)	541	245.9	240.7	244.7	250.1	244.8	247.1

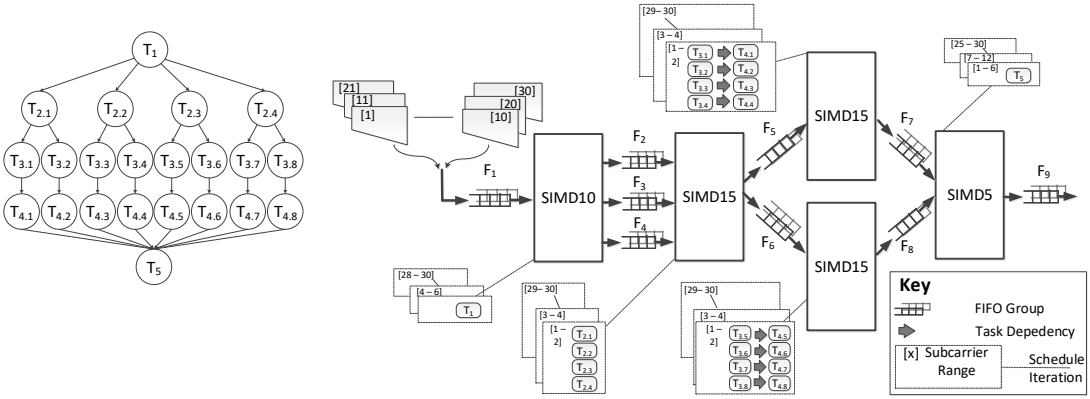

(a) Dataflow (b) Architecture

Fig. 21: Architecture Synthesis of 2×2 R-BSFE 16-QAM, $\tilde{m} = [1, 1, 2, 4]$ based on [40]

This trend continues in Table IV. Comparing three configurations of BSS-EFE to R-BSFE, R-BSFE never incurs a greater DSP48E1 cost, offers the same performance and always offers superior throughput. BFSD reduces LUT cost, but requires more DSPs than R-BSFE-$[1, 1, 1, 4]$.

Recall, though, that the R-BSFE configurations were chosen to most closely match those of BSS-EFE configurations to which they were compared; this comparison neglects to consider R-BSFE configurations which cannot be approximated by BSS-EFE. For instance, compare BSS-EFE-$[1, 1, 4, 12]$ with three R-BSFE configurations, illustrated in Fig. 22, with accelerator metrics as quoted in Table V.

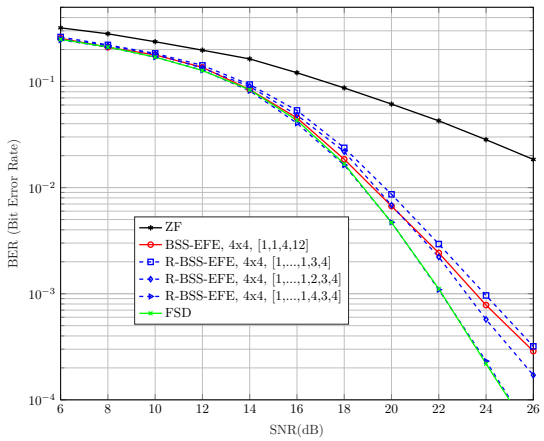

Fig. 22: Performance Comparison: R-BSFE v.s. BSS-EFE and FSD, 4×4 16-QAM

As shown in Fig. 22, R-BSFE-$[1, ..1, 4, 3, 4]$ enables generally superior detection accuracy to BSS-EFE-$[1, 1, 4, 12]$ at SNR above 14 dB. R-BSFE-$[1, ..1, 2, 3, 4]$ enables almost identical accuracy and, for most practical purposes (i.e. SNR below 14 dB), the accuracy of each of these three are indistinguishable. However, the accelerator cost of the R-BSFE solutions is significantly lower. Relative to BSS-EFE-$[1, 1, 4, 12]$, R-BSFE-$[1, 1, 1, 1, 2, 3, 4]$ consumes 27% fewer DSP48E1 slices and 46.7% fewer LUTs. It also enables peak throughput 7% higher than BSS-EFE-$[1, 1, 4, 12]$. The key benefit of R-BSFE is in allowing more fine-grained control of SD complexity to balance complexity and detection accuracy between quasi-optimal and across the sub-optimal range, resulting in less complex implementations for real-time SD.

TABLE V: Resource Comparison: R-BSFE v.s. BSS-EFE and FSD, 4×4, 16-QAM

Detector	FSD [40]	BSS-EFE [41]	R-BSFE	
Configuration	N/A	[1,1,4,12]	$[1, ..., 1, 4, 3, 4]$	$[1, ..., 1, 2, 3, 4]$
DSP48E1	216	495	573	360
LUT ($\times 10^3$)	31.1	112.6	77.4	60.1
BRAM	0	0	0	0
Clock (MHz)	298	252	247	305
T (Mbps)	483.2	484.8	481.65	519.14

The performance of R-BSFE-$\tilde{\mathbf{m}} = [1, ..., 1, 2, 8]$ is as shown in Fig. 23. When compared with K-BEST ($K = 8$), chosen because of its similar detection performance for 64-QAM 4×4 MIMO [33], it offers almost identical performance but the resulting accelerator for R-BSFE requires 30% fewer LUT and 76% fewer DSP resources, as quoted in Table VI.

IX. Conclusion

Modern MIMO systems vary dramatically in scale and complexity, with standards commonly supporting antenna topologies varying from 2×2 - 8×8 and modulation densities of QPSK - 1024-QAM. Baseband signal processing operations such as symbol detection need to be able to adapt not only to these requirements, but also

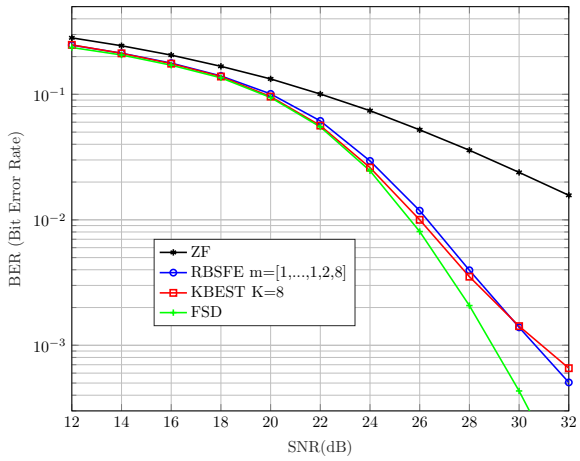

Fig. 23: Performance comparison: R-BSFE v.s. K-BEST and FSD, 4×4,64-QAM

TABLE VI: Resource comparison: R-BSFE v.s. K-BEST and FSD, 4×4, 64-QAM

Detector	FSD [40]	K-BEST [33]	R-BSFE
Configuration	N/A	K=8	$[1, ..., 1, 2, 8]$
DSP48E1	304	565	188
LUT ($\times 10^3$)	154.42	81.45	50.00
Clock (MHz)	278	167	309
T (Mbps)	506.4	501	494

to supporting devices with differing levels of performance, cost and power consumption.

This paper presented a novel configurable SD for this purpose. R-BSFE supports varying levels of symbol detection accuracy and cost. It employs a novel real-valued symbol enumeration approach which selects, for any user-defined number of enumerated symbols, the most likely candidates from the QAM constellation. This is combined with a novel pre-processing approach to ordering the columns of the channel matrix for detection which accounts for the structure of the SD tree to order the antennas differently, based on the specific configuration. Combined, these increase detection accuracy by up to 9 dB whilst maintaining quasi-ML accuracy with roughly equal complexity. However, the real-valued enumeration approach makes available configurations which would not otherwise be possible, which enables similar or better accuracy than the state of the art, with higher throughput and considerable reduced cost. For instance when R-BSFE accelerators on Xilinx FPGA are compared to those for BSS-EFE, complexity reductions of up to 42% lead to throughput increases of up to 7% and FPGA resource cost reductions of up to 46.5% whilst increasing accuracy.

References

[1] A. Sibille, C. Oestges, and A. Zanella, *MIMO: From Theory to Implementation*, 1st ed. Academic Press, 2010.

[2] E. Dahlman, S. Parkvall, and J. Skold, *4G LTE/LTE-Advanced for Mobile Broadband*, 1st ed. Academic Press, 2011.

[3] Rohde & Schwarz, "WLAN 802.11n: from SISO to MIMO," Mühldorfstraße 15 — D - 81671 München, Application Note, 2011.

[4] ——, "802.11ac technology introduction," Mühldorfstraße 15 — D - 81671 München, White Paper, 2013.

[5] ——, "802.11ax technology introduction," Mühldorfstraße 15 — D - 81671 München, White Paper, 2016.

[6] A. Gohil, H. Modi, and S. K. Patel, "5G technology of mobile communication: A survey," in *2013 Int. Conf. on Intelligent Inf.and Signal Process. (ISSP)*, March 2013, pp. 288–292.

[7] A. Al-Fuqaha, M. Guizani, M. Mohammadi, M. Aledhari, and M. Ayyash, "Internet of things: A survey on enabling technology, protocols, and applications," *IEEE Commun. Surveys Tutorials*, vol. 17, no. 4, pp. 2347–2376, Fourthquarter 2015.

[8] S. Yang and L. Hanzo, "Fifty years of MIMO detection: The road to large-scale MIMOs," *IEEE Commun. Surveys Tutorials*, vol. 17, no. 4, pp. 1941–1988, Fourthquarter 2015.

[9] C. P. Schnorr and M. Euchner, "Lattice basis reduction: Improved practical algorithms and solving subset sum problems," *J. Mathematical Programming*, vol. 66, no. 1, pp. 181–199, Aug 1994. [Online]. Available: https://doi.org/10.1007/BF01581144

[10] A. Klein, G. K. Kaleh, and P. W. Baier, "Zero forcing and minimum mean-square-error equalization for multiuser detection in code-division multiple-access channels," *IEEE Trans. Veh. Technol.*, vol. 45, no. 2, pp. 276–287, May 1996.

[11] X. Nguyen, M. Le, N. Pham, and V. Ngo, "A pipelined schnorr-euchner sphere decoder architecture for MIMO systems," in *2015 Int. Conf. on Advanced Technol. for Commun. (ATC)*, Oct 2015, pp. 366–371.

[12] X. Liang, H. Zhou, Z. Zhang, X. You, and C. Zhang, "Joint list polar decoder with successive cancellation and sphere decoding," in *2018 IEEE Int. Conf. on Acoust., Speech and Signal Process. (ICASSP)*, April 2018, pp. 1164–1168.

[13] A. Burg, M. Borgmann, M. Wenk, M. Zellweger, W. Fichtner, and H. Bolcskei, "VLSI implementation of MIMO detection using the sphere decoding algorithm," *IEEE J. Solid-State Circuits*, vol. 40, pp. 1566 – 1577, 08 2005.

[14] A. Wiesel, X. Mestre, A. Pages, and J. R. Fonollosa, "Efficient implementation of sphere demodulation," in *2003 4th IEEE Workshop on Signal Process. Advances in Wireless Commun. - SPAWC 2003 (IEEE Cat. No.03EX689)*, June 2003, pp. 36–40.

[15] C. Liao, T. Wang, and T. Chiueh, "A 74.8 mw soft-output detector ic for 8 ×8 spatial-multiplexing MIMO communications," *IEEE J. Solid-State Circuits*, vol. 45, no. 2, pp. 411–421, 2010.

[16] J. Jalden, L. G. Barbero, B. Ottersten, and J. S. Thompson, "The error probability of the fixed-complexity sphere decoder," *IEEE Trans. Signal Process.*, vol. 57, no. 7, pp. 2711–2720, 2009.

[17] I. A. Bello, B. Halak, M. El-Hajjar, and M. Zwolinski, "VLSI implementation of a scalable k-best MIMO detector," in *2015 15th Int. Symp. on Commun. and Inf. Technol. (ISCIT)*, Oct 2015, pp. 281–286.

[18] R. E. Chall, F. Nouvel, M. Hélard, and M. Liu, "Iterative receivers combining MIMO detection with turbo decoding: performance-complexity trade-offs," *EURASIP J. on Wireless Commun. and Networking*, vol. 2015, no. 1, p. 69, Mar 2015. [Online]. Available: https://doi.org/10.1186/s13638-015-0305-6

[19] Y. Wu and J. McAllister, "Bounded selective spanning with extended fast enumeration for MIMO-OFDM systems detection," in *21st European Signal Process. Conf. (EUSIPCO 2013)*, Sept 2013, pp. 1–5.

[20] B. M. Hochwald and S. Ten Brink, "Achieving near-capacity on a multiple-antenna channel," *IEEE Trans. Commun.*, vol. 51, no. 3, pp. 389–399, 2003.

[21] V. Bhojak and A. Sharma, "MIMO wireless systems: V-blast architecture," in *2013 Third Int. Conf. on Advanced Comput. and Commun. Technol. (ACCT)*, April 2013, pp. 215–220.

[22] E. Larsson, "MIMO detection methods: How they work [lecture notes]," *IEEE Signal Process. Mag.*, vol. 26, no. 3, pp. 91–95, May 2009.

[23] M. O. Damen, H. E. Gamal, and G. Caire, "On maximum-likelihood detection and the search for the closest lattice point," *IEEE Trans. on Inf. Theory*, vol. 49, no. 10, pp. 2389–2402, Oct 2003.

[24] T.-D. Chiueh, P.-Y. Tsai, and I.-W. Lai, *Baseband Receiver Design for Wireless MIMO-OFDM Communication*, 2nd ed. Wiley-IEEE Press, 2012.

[25] D. Wubben, R. Bohnke, J. Rinas, V. Kuhn, and K. D. Kammeyer, "Efficient algorithm for decoding layered space-time codes," *Electronics Letters*, vol. 37, no. 22, pp. 1348–1350, 2001.

[26] T.-D. Chiueh and P.-Y. Tsai, *OFDM Baseband Receiver Design for Wireless Communications*. Wiley Publishing, 2007.

[27] B. Mennenga and G. Fettweis, "Search sequence determination for tree search based detection algorithms," in *2009 IEEE Sarnoff Symp.*, 2009, pp. 1–6.

[28] B. Hassibi and H. Vikalo, "On the sphere-decoding algorithm i. expected complexity," *IEEE Trans. on Signal Process.*, vol. 53, no. 8, pp. 2806–2818, Aug 2005.

[29] M. Mohammadkarimi, M. Mehrabi, M. Ardakani, and Y. Jing, "Deep learning-based sphere decoding," *IEEE Trans. Wireless Comm.*, vol. 18, no. 9, pp. 4368–4378, 2019.

[30] Z. Liang, D. Lv, C. Cui, H. B. Chen, W. He, W. Sheng, N. Jing, Z. Mao, and G. He, "A 3.85-gb/s 8x 8 soft-output MIMO detector with lattice-reduction-aided channel preprocessing," *IEEE Trans. on Very Large Scale Integration (VLSI) Syst.*, pp. 1–14, 2020.

[31] X. Chu and J. McAllister, "FPGA based soft-core SIMD processing: A MIMO-OFDM fixed-complexity sphere decoder case study," in *2010 International Conference on Field-Programmable Technology*, 2010, pp. 479–484.

[32] Z. Guo and P. Nilsson, "Algorithm and implementation of the k-best sphere decoding for MIMO detection," *IEEE J. Sel. Areas Commun.*, vol. 24, no. 3, pp. 491–503, March 2006.

[33] T. Hanninen, M. S. Saud, H. Y. Amin, and M. Juntti, "MIMO detector implementations using high-level synthesis tools from different generations," in *2017 51st Asilomar Conf. on Signals, Syst., and Comput.*, 2017, pp. 489–493.

[34] A. Shirly Edward and S. Malarvizhi, "Architectural implementation of modified k-best algorithm for detection in MIMO systems," *J. Microprocessors and Microsystems*, vol. 74, p. 103010, 2020. [Online]. Available: http://www.sciencedirect.com/science/article/pii/S0141933117303691

[35] M. Li, B. Bougard, E. E. Lopez, A. Bourdoux, D. Novo, L. V. D. Perre, and F. Catthoor, "Selective spanning with fast enumeration: A near maximum-likelihood MIMO detector designed for parallel programmable baseband architectures," in *2008 IEEE Int. Conf. on Commun.*, May 2008, pp. 737–741.

[36] S. A. Joshi, T. S. Rukmini, and H. M. Mahesh, "Error rate analysis of the V-BLAST MIMO channels using interference cancellation detectors," in *2011 Int. Conf. on Signal Process., Commun., Comput. and Netw. Technol.*, July 2011, pp. 614–618.

[37] U. Fincke, "Improved methods for calculating vectors of short length in a lattice, including a complexity analysis," vol. 44, pp. 463–471, 04 1985.

[38] H. Lee, K. Oh, M. Cho, Y. Jang, and J. Kim, "Efficient low-latency implementation of CORDIC-based sorted qr decomposition for multi-gbps MIMO systems," *IEEE Trans. Circuits Syst., II, Exp. Briefs*, vol. 65, no. 10, pp. 1375–1379, 2018.

[39] C. Zheng, X. Chu, J. McAllister, and R. Woods, "Real-valued fixed-complexity sphere decoder for high dimensional QAM-MIMO systems," *IEEE Trans. Signal Process.*, vol. 59, no. 9, pp. 4493–4499, 2011.

[40] Y. Wu and J. McAllister, "Architectural synthesis of multi-SIMD dataflow accelerators for FPGA," *IEEE Trans. Parallel Distrib. Syst.*, vol. 29, no. 1, pp. 43–55, Jan 2018.

[41] Y. Wu and J. McAllister, "Bounded selective spanning with extended fast enumeration for MIMO-OFDM systems detection," *IEEE Trans. Circuits Syst.I, Reg. Papers*, vol. 64, no. 9, pp. 2556–2568, Sept 2017.